LAPEENRANTA UNIVERSITY OF TECHNOLOGY

FACULTY OF TECHNOLOGY

Master's Degree Programme in Technomathematics and Technical Physics

FABRICATION TECHNOLOGY AND APPLICATIONS OF FIBER BRAGG GRATINGS

Examiners: Professor, D.Sc., Erkki Lähderanta
Professor, D.Sc., Oleg G. Okhotnikov
Supervisors: Professor, D.Sc., Erkki Lähderanta
Professor, D.Sc., Oleg G. Okhotnikov

Lappeenranta 2008

Regina Gumenyuk
Orivedenkatu 8 A 15
33720 Tampere
Phone: +358449480919

ABSTRACT

LAPPEENRANTA UNIVERSITY OF TECHNOLOGY
FACULTY OF TECHNOLOGY
Master's Degree Programme in Technomathematics and Technical Physics

Regina Gumenyuk

Fabrication technology and applications of fiber Bragg gratings.

Master's Thesis

2008

52 pages, 35 figures, 3 tables and 1 appendix.

Examiners: Professor, Oleg Okhotnikov
Professor, Erkki Lähderanta
Keywords: FBG, photosensitivity, phase mask technique, hydrogen loading, strain and temperature sensors.

In this thesis theoretical and technological aspects of fiber Bragg gratings (FBG) are considered. The fabrication of uniform and chirped fiber Bragg gratings using phase mask technique has been exploited throughout this study. Different requires of FBG inscription were considered and implemented experimentally to find economical and effective procedure. The hydrogen loading was used as a method for enhancement the photosensitivity of the fiber. The minimum loading time for uniform and chirped fiber Bragg gratings was determined as 3 days and 7 days at T = 50°C and hydrogen pressure 140 bar, respectively. The post-inscription annealing was considered to avoid excess losses induced by the hydrogen. The wavelength evolution during annealing was measured.

The strain and temperature sensor application of FBG was considered. The wavelength shifts caused by tension and temperature were studied for both uniform and chirp fiber Bragg gratings.

PREFACE

This work has been carried out at Optoelectronics Research Centre of Tampere University of Technology.

I wish to thank Professor Marcus Pessa for giving me opportunity to write diploma work here.

I wish to express my deepest gratitude to Professor Oleg Okhotnikov for his support and guidance. Without his help this work would not be possible. In particular, I would like to thank Samuli Kivistö. He has helped me a lot during the writing of my diploma work.

I wish to express my gratitude to Professors Erkki Lähderanta and Sergey Karmamenko for their support during my studies at LUT.

Big thanks belong to the Professor's stuff of Microelectronics Department of Saint-Petersburg State Electrotechnical University "LETI" for giving high-quality of education and support during my studies.

Especially, I wish to thank my mum for her supporting.

Lappeenranta, May 2008
Regina Gumenyuk

CONTENTS

ABBREVIATIONS AND SYMBOLS

Roman lettes

E	Electric field vector
H	Magnetic field vector
D	Electric flux density
B	Magnetic flux density
t	Time
P	Induced electric polarization
M	Induced magnetic polarization
$\widetilde{E}$	Fourier transform of E
$\widetilde{P}$	Fourier transform of P
n	Refractive index
k_0	Free space wave number
J_m, K_m	Bessel functions
a	Core radius
m	Integer
n_1	Refractive index of core
n_2	Refractive index of cladding
V	Normalized frequency
b	Propagation constant
$\overline{n}$	Modal refractive index
T	Delay time
L	Fiber length
ΔT	Pulse broadening
D	Dispersion parameter
D_M	Material dispersion
D_W	Waveguide dispersion
k_i	Incident wave vector
k_f	Scattered wave vector
K	Grating wave vector
g	Apodization function
R	Reflectivity at line center
C	Hydrogen concentration

D	Diffusion coefficient
D_0	Frequency factor
E_d	Activation energy
T	Temperature
R	Gas constant
B	Grating length

Greek lettes

ε_0	Permittivity in vacuum
μ_0	Permeability in vacuum
χ	Susceptibility
$\widetilde{\chi}$	Fourier transform of χ
ω	Frequency
λ	Wavelength
β	Propagation constant
Δ	Index difference
v_g	Group velocity
$\Delta\omega$	Spectral width of the pulse
β_2	GVD parameter
$\Delta\lambda$	Wavelength bandwidth
n_{2g}	Group index of the cladding material
λ_{ZD}	Zero-dispersion wavelength
λ_B	Bragg wavelength
n_{eff}	Modal index
Λ	Grating period
ω_f	Frequency of the incident radiation
ω_i	Frequency of the reflected radiation
δn	Index perturbation
r	Local reflectivity
ρ	Reflectivity
κ	Coupling coefficient
η	Modal overlap factor

δn_{eff}	Chirp
n'_{eff}	Modal index of the grating-coupled reflected (a negative quantity) or transmitted wave
Ω	Coupling coefficient for the sinusoidal refractive index modulation
ϕ	Function of local phase of the chirped grating
ε	Longitudinal strain
ρ_{α}	Photoelastic coefficient of the fiber
ρ_{11} , ρ_{12}	Components of the fiber-optic strain tensor
ν	Poisson's ratio
δb	Reflection location
ς	Constant determined by the photoelastic properties of the fiber
λ_{B1}	Boundary wavelength of CFBG from the short wavelength side
λ_{B2}	Boundary wavelength of CFBG from the long wavelength side
$\Delta\lambda_C$	Difference boundary CFBG wavelengths
$\Delta\lambda_{BT}$	Wavelength shift corresponding temperature change
ξ	Fiber thermo-optic coefficient

Abbreviations

FBG	Fiber Bragg grating
dB	Decibel
LAN	Local area network
UFBG	Uniform fiber Bragg grating
CFBG	Chirped fiber Bragg grating
HE	Hybrid modes of electric and magnetic field
TE	Transverse electric mode
GVD	Group-velocity dispersion
UV	Ultraviolet
MCVD	Modified chemical vapor deposition
SMF	Single-mode fiber
WDM	Wavelength-division multiplexing
ASE	Amplified spontaneous emission

1 INTRODUCTION

The phenomenon of total internal reflection, responsible for guiding of light in optical fiber, has been known since 1854. Although first samples of glass fibers were made in the 1920s, their use became practical only in the 1950s. During the following 20 years they were used mainly for medical imaging over short distances and were not considered for communication purposes because of high losses (~ 1000 dB/km). The situation changed dramatically in 1970 when the losses of optical fibers were reduced to 20 dB/km and during next 9 years down to 0.2 dB/km at the 1.55 μm spectral range. The availability of low-loss fibers led to a revolution in the field of lightwave technology and started the era of fiber-optic communications [1].

There are two basic fiber types: multimode fiber and single-mode fiber. Multimode fiber is used for short transmission distances, e.g. local area network (LAN) systems and video surveillance. Single mode fiber is suitable for long transmission distances, typical in long-distance telephony and multichannel television broadcast system [2].

Multimode fibers have core diameters typically ranged from 50 to 105 μm. Light propagates in these fibers in the form of multiple modes, each having slightly different path through the fiber and thus effectively traveling at a slightly different velocity. As a result, the short optical pulse broadens after propogation along the fiber. This phenomenon is known as dispersion, and this specific form is called modal dispersion [3].

Single-mode optical fiber has relatively small core diameter of 4 - 10 μm. It guides all the energy in the form of a single spatial mode and, therefore, the modal dispersion is not in the play. It has low attenuation and allows for high capacity data transmission.

Discovery of the fiber photosensitivity has opened up new possibilities. The photosensitivity allows to fabricate fiber Bragg gratings (FBG), which are now widely used in many applications such as multiplexers, demultiplexsers and add/drop filters, where individual wavelength selection and separation is required. The most developed sphere of FBG application is sensing. FBG sensors have found various applications for monitoring of civil and industrial engineering structures. They are used to monitor strain stuck on the structure parameters, e.g. acceleration, pressure, ultrasound, high magnetic field and force. FBG sensors have a number of distinguishing advantages [4]. (1) Their parameters are insensitive

to fluctuations in the power of the ligth source. The information contains in the wavelength shift induced by external influence. (2) They can be directly written into the fiber, which makes them compatible with wide range of devices using small diameter probes. (3) They can be produced in volume at low cost, making them competitive with conventional electrical sensors. For fabricating FBG sensor the single-mode fiber is usually used.

In this thesis I describe the fabrication technology of uniform fiber Bragg gratings (UFBG) and chirped fiber Bragg gratings (CFBG). The main attention was put on the improvement of FBG characteristics using organized hydrogen loading and thermal annealing. The temperature and strain sensor application of FBG were also considered.

The thesis consists of 4 chapters. In the chapter 2 theoretical grounds of single-mode fibers and fiber Bragg gratings are presented. In chapter 3 I describe the fabrication technology of FBG and the workstation used in this study. The hydrogen loading technique and annealing process has been described in detail. In the chapter 4 I present the result of strain and temperature measurements using UFBG and CFBG.

2 BASIC PROPERTIES OF SINGLE-MODE OPTICAL FIBERS AND FIBER BRAGG GRATINGS

Typical optical fiber consists of a cylindrical core of silica glass, surrounded by a cladding and jacket, being for protection of previous layers. The refractive index of cladding is lower than that of the core, thereby providing the total internal reflection. Because of index change at the core-cladding interface there are two types of fibers: step-index and graded-index fibers (Fig. 1).

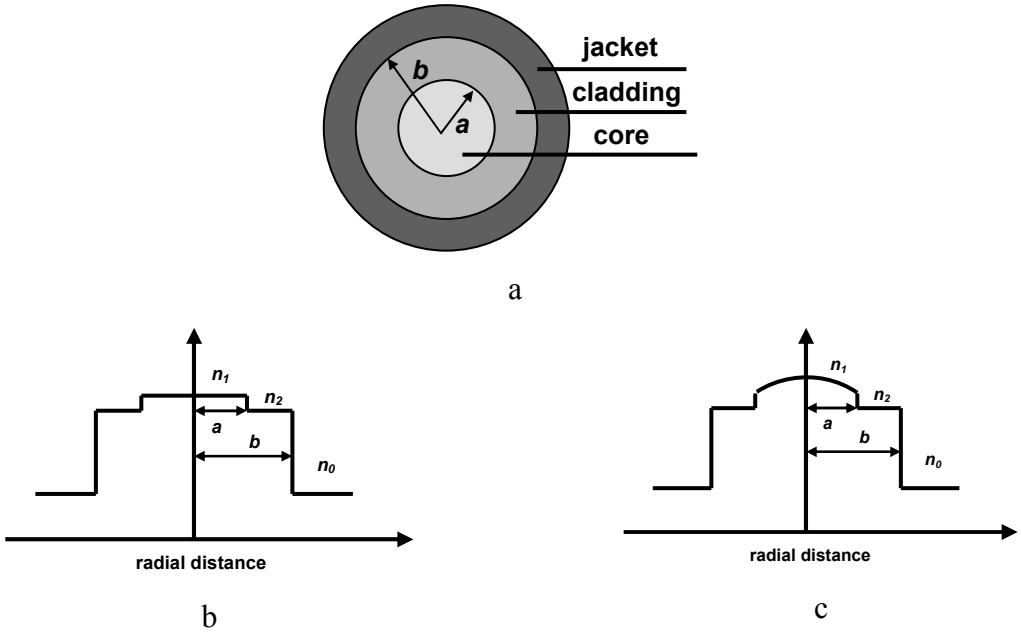

Fig. 1. Cross section of optical fiber (a); refractive index profile for step-index (b) and graded-index fibers (c).

In this chapter I consider the basic principles of light propagation, properties of the single-mode fiber and characteristics of fiber Bragg gratings.

2.1 Single-mode optical fibers

2.1.1 Light propagation in optical fibers

Light propagation is described by Maxwell's equations. For a nonconducting medium without free charges, these equations take the form

$$\nabla \times \boldsymbol{E} = -\partial \boldsymbol{B} / \partial t , \tag{2.1}$$

$$\nabla \times \boldsymbol{H} = \partial \boldsymbol{D} / \partial t , \tag{2.2}$$

$$\nabla \cdot \boldsymbol{D} = 0\,, \tag{2.3}$$

$$\nabla \cdot \boldsymbol{B} = 0\,, \tag{2.4}$$

where $\boldsymbol{E}$ and $\boldsymbol{H}$ are the electric and magnetic field vectors, respectively, and $\boldsymbol{D}$ and $\boldsymbol{B}$ are corresponding flux densities. The flux densities have the following relation to electric and magnetic field:

$$\boldsymbol{D} = \varepsilon_0 \boldsymbol{E} + \boldsymbol{P}\,, \tag{2.5}$$

$$\boldsymbol{B} = \mu_0 \boldsymbol{H} + \boldsymbol{M}\,, \tag{2.6}$$

where ε_0 is the permittivity in vacuum, μ_0 is the permeability in vacuum, and $\boldsymbol{P}$ and $\boldsymbol{M}$ are the induced electric and magnetic polarizations, respectively. For optical fibers $\boldsymbol{M}$ = 0 because of nonmagnetic nature of silica glass.

By taking the curl of equation (2.1) and using Eqs. (2.2), (2.5) and (2.6) we get the wave equation

$$\nabla \times \nabla \times \nabla \boldsymbol{E} = -\mu_0 \varepsilon_0 \frac{\partial^2 \boldsymbol{E}}{\partial t^2} - \mu_0 \frac{\partial^2 \boldsymbol{P}}{\partial t^2}\,. \tag{2.7}$$

The equation (2.7) can be solved using Fourier transforms and then **E** can be defined as

$$\boldsymbol{E}(\boldsymbol{r},t) = \frac{1}{2\pi} \int_{-\infty}^{\infty} \tilde{\boldsymbol{E}}(\boldsymbol{r},\omega) \exp(-i\omega t) d\omega\,, \tag{2.8}$$

where $\tilde{\boldsymbol{E}}(\boldsymbol{r},\omega)$ is the Fourier transform of $\boldsymbol{E}$.

The equation (2.7) in frequency domain takes the form

$$\nabla \times \nabla \times \nabla \tilde{\boldsymbol{E}} = \mu_0 \varepsilon_0 \omega^2 \tilde{\boldsymbol{E}} + \mu_0 \omega^2 \tilde{\boldsymbol{P}}\,. \tag{2.9}$$

$\tilde{\boldsymbol{P}}$ can be expressed in term of $\tilde{\boldsymbol{E}}$ according to the relation

$$\widetilde{\boldsymbol{P}}(\boldsymbol{r},\omega)=\varepsilon_0\widetilde{\chi}(\boldsymbol{r},\omega)\widetilde{\boldsymbol{E}}(\boldsymbol{r},\omega)\,, \tag{2.10}$$

where $\widetilde{\chi}(\boldsymbol{r},\omega)$ is Fourier transform of susceptibility χ and is related to refractive index by the relation $n(\omega)=\sqrt{1+\widetilde{\chi}(\omega)}$. According to these ratios and by using the identity

$$\nabla\times\nabla\times\widetilde{\boldsymbol{E}}=\nabla(\nabla\cdot\widetilde{\boldsymbol{E}})-\nabla^2\widetilde{\boldsymbol{E}}\,, \tag{2.11}$$

the Eq. (2.9) can be rewritten as

$$\nabla^2\widetilde{\boldsymbol{E}}+n^2(\omega)k_0^2\widetilde{\boldsymbol{E}}=0\,, \tag{2.12}$$

where $k_0=2\pi/\lambda$ is wave number in free space.

In a consequence of algebraic solutions we get the following eigenvalue equation

$$\left[\frac{J_m'(pa)}{pJ_m(pa)}+\frac{K_m'(qa)}{qK_m(qa)}\right]\cdot\left[\frac{J_m'(pa)}{pJ_m(pa)}+\frac{n_2^2}{n_1^2}\frac{K_m'(qa)}{qK_m(qa)}\right]=\frac{m^2}{a^2}\left(\frac{1}{p^2}+\frac{1}{q^2}\right)\left(\frac{1}{p^2}+\frac{n_2^2}{n_1^2}\frac{1}{q^2}\right), \tag{2.7}$$

where J_m and K_m are different kinds of Bessel functions; a is core radius; p and q are parameters, which can be defined by

$$p^2=n_1^2k_0^2-\beta^2\,, \tag{2.8}$$

$$q^2=\beta^2-n_2^2k_0^2\,, \tag{2.9}$$

where β is propagation constant, n_1 and n_2 are refractive index of core and cladding, respectively.

For given parameters k_0, a, n_1 and n_2, the eigenvalue equation (2.7) can be solved numerically to determine the propagation constant β. This constant defines a certain mode guided in fiber.

Single-mode fibers support only the HE_{11} mode called fundamental mode of the fiber. The fiber is designed in such a way that all higher-order modes are cut off at the operating wavelength. A parameter that plays an important role in determining the cutoff condition is defined as

$$V = k_0 a (n_1^2 - n_2^2)^{1/2} \approx (2\pi/\lambda) a n_1 \sqrt{2\Delta} \,. \tag{2.10}$$

It is called the normalized frequency or simply the V parameter. It is also useful to introduce a normalized propagation constant b as

$$b = \frac{\beta / k_0 - n_2}{n_1 - n_2} = \frac{\bar{n} - n_2}{n_1 - n_2} \,. \tag{2.11}$$

Single-mode condition can be determined by the value of V at which the TE_{01} (Transverse Electric, which has no electric field in the direction of propagation.) and TM_{01} (Transverse Magnetic, which has no magnetic field in the direction of propagation) modes can not be guided. The eigenvalue equations for these modes are obtained by setting m=0 in Eq. (2.7) and are given by:

$$pJ_0(pa)K_0'(qa) + qJ_0'(pa)K_0(qa) = 0 \,, \tag{2.12}$$

$$pn_2^2 J_0(pa)K_0'(qa) + qn_1^2 J_0'(pa)K_0(qa) = 0 \,. \tag{2.13}$$

A mode reaches cutoff when q=0. Since pa=V when q=0, the cutoff condition for both modes is simply given by $J_0(V) = 0$ and the smallest value of V for this equation is 2.405. A fiber designed so that V<2.405 supports only the fundamental HE_{11} (which has both electric and magnetic field components in the direction of propagation) mode. This is condition for the single-mode propogation. Note that V decreases with a and $\Delta = (n_1 - n_2)/n_1$. Thus single-mode fibers typically have small radius and differences of core-cladding refractive index, e.g. a = 4μm and Δ = 0.003.

The modal refractive index $\bar{n}$ at the operating wavelength can be obtained by using Eq. (2.11):

$$\overline{n} = n_2 + b(n_1 - n_2) \approx n_2(1 + b\Delta)\,. \tag{2.14}$$

The axial components E_z and H_z are quite small for $\Delta << 1$. Hence, the HE_{11} mode is linearly polarized for weakly guiding fibers. One of the transverse components can be neglected for linearly polarized mode. If we set $E_y = 0$, the E_x component of the electric field for HE_{11} mode is given by

$$E_x = E_0 \begin{cases} [J_0(p\rho)/J_0(pa)]\exp(i\beta z); & \rho \le a, \\ [K_0(q\rho)/K_0(qa)]\exp(i\beta z); & \rho > a, \end{cases} \tag{2.15}$$

where E_0 is an amplitude of the mode field. The dominant component of the corresponding magnetic field is given by $H_y = n_2(\varepsilon_0/\mu_0)^{1/2} E_x$. This mode is linearly polarized along the *x* axis. The same fiber supports another mode linearly polarized along the *y* axis. In this case a single-mode fiber actually supports two orthogonally polarized modes that are degenerate and have the same mode index [2, 3].

2.1.2 Fiber dispersion

Dispersion describes the effect when different spectral components of the transmitted signal travel with the different velocities in an optical fiber. The main advantage of single-mode fibers is that intermodal dispersion is absent cause of the entire energy of the injected optical pulse is transported solely by a single mode. However, the pulse broadening could still be observed. The group velocity associated with the fundamental mode is frequency dependent resulting in the chromatic dispersion. As a consequence, different spectral components of the pulse travel at slightly different group velocities. This phenomenon is known as group-velocity dispersion (GVD), intramodal dispersion, or simply fiber dispersion. Intramodal dispersion has two contributions, material dispersion and waveguide dispersion [2, 3].

Group-velocity dispersion

Let us consider a single-mode fiber of length *L*. A specific spectral component at the frequency ω would arrive at the output end of the fiber after delay $T = L/v_g$, where v_g is the group velocity and it can be defined as

$$v_g = (d\beta / d\omega)^{-1}. \tag{2.16}$$

Since the different spectral components of the pulse disperse during the propagation they appear at the fiber output at different times, resulting in the pulse broadening. If $\Delta\omega$ is the spectral width of the pulse, the pulse broadening for fiber of length L is

$$\Delta T = \frac{dT}{d\omega}\Delta\omega = \frac{d}{d\omega}\left(\frac{L}{v_g}\right)\Delta\omega = L\frac{d^2\beta}{d\omega^2}\Delta\omega = L\beta_2\Delta\omega, \tag{2.17}$$

The parameter $\beta_2 = d^2\beta / d\omega^2$ is known as the GVD parameter. It determines how much an optical pulse would broaden during propagation through the fiber.

Eq. (2.17) can be written in terms of $\Delta\lambda$ emitted by optical source using $\omega = 2\pi c / \lambda$ and $\Delta\omega = (-2\pi c / \lambda^2)\Delta\lambda$:

$$\Delta T = \frac{d}{d\lambda}\left(\frac{L}{v_g}\right)\Delta\lambda = DL\Delta\lambda, \tag{2.18}$$

where

$$D = \frac{d}{d\lambda}\left(\frac{1}{v_g}\right) = -\frac{2\pi c}{\lambda^2}\beta_2 \tag{2.19}$$

is the dispersion parameter expressed in units of ps/(km-nm).

The wavelength dependence of D is governed by the frequency dependence of the mode index $\overline{n}$. From Eq. (2.19) D can be written as

$$D = -\frac{2\pi c}{\lambda^2}\frac{d}{d\omega}\left(\frac{1}{v_g}\right) = -\frac{2\pi}{\lambda^2}\left(2\frac{d\overline{n}}{d\omega} + \omega\frac{d^2\overline{n}}{d\omega^2}\right). \tag{2.20}$$

By using Eq. (2.10) and substituting $\overline{n}$ from Eq. (2.14), D can be presented as the sum of two terms

$$D = D_M + D_W \,, \tag{2.21}$$

where the material dispersion D_M and the waveguide dispersion D_W are given by

$$D_M = -\frac{2\pi}{\lambda^2}\frac{dn_{2g}}{d\omega} = \frac{1}{c}\frac{dn_{2g}}{d\lambda} \,, \tag{2.22}$$

$$D_W = -\frac{2\pi\Delta}{\lambda^2}\left[\frac{n_{2g}^2}{n_2\omega}\frac{Vd^2(Vb)}{dV^2} + \frac{dn_{2g}}{d\omega}\frac{d(Vb)}{dV}\right]. \tag{2.23}$$

Here n_{2g} is the group index of the cladding material and the parameters V and b are given by Eqs. (2.10) and (2.11) [2].

The mechanism for material dispersion is based on the dependence in refractive index on the optical frequency ω. On fundamental level, the origin of material dispersion is related to the characteristic resonance frequencies at which the material absorbs the electromagnetic radiation. When $dn_{2g}/d\lambda = 0$, D_M is equal to zero. This wavelength is referred to as the zero-dispersion wavelength λ_{ZD} [2].

The waveguide dispersion originates from the dependence of power distribution on the wavelength. The light energy of a mode propagates partly in the core and partly in the cladding consequently. The effective index of a mode has the value between the refractive indices of the cladding and the core. The actual value of effective index depends on the ratio of power that is contained in the cladding and in the core. If most of the power propagates in the cladding, the effective index is closer to the cladding refractive index. If most of the power is confined within in the core, the effective index is closer to the core refractive index. The power ratio in the between core and cladding of the fiber is a function of wavelength. Thus, if the wavelength changes, the power distribution changes and the effective index or propagation constant of the mode changes too [3].

Fig. 2 shows D_M and D_W, and their sum $D = D_M + D_W$, for a typical single-mode fiber. The waveguide dispersion shifts λ_{ZD} by amount of 30 - 40 nm to longer wavelength resulting $\lambda_{ZD} = 1.31$ μm.

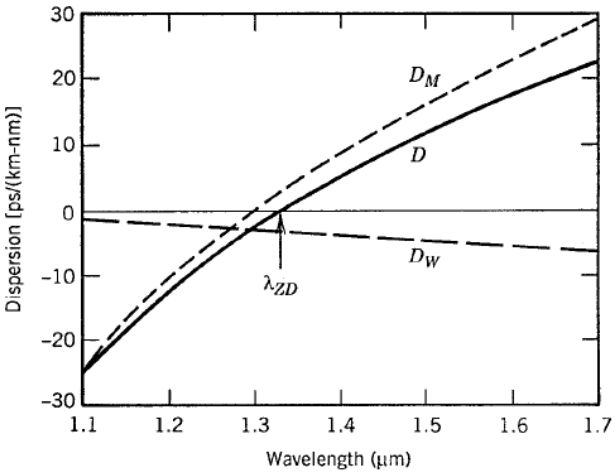

Fig. 2. Total dispersion D and relative contributions of material dispersion D_M and waveguide dispersion D_W for a single-mode fiber.

By varying the dispersion parameters, different kinds of fibers can be obtained. The dispersion management is used largely at $\lambda \sim 1.5$ μm wavelength range exploited in optical communication. Since the contribution D_W depends on fiber core a and the index difference Δ, it is possible to design a fiber in such was that λ_{ZD} could be significantly shifted. Such fibers are called dispersion-shifted fibers. It is possible also to make the waveguide contribution so that the total dispersion D is relatively small over a wide wavelength range. Such fibers are called dispersion-flattened fibers. If the fiber consists of GVD decreasing along the fiber length because of axial variations in the core radius, this is dispersion-decreasing fiber. If GVD is made normal and has a relatively large magnitude, such fibers are called dispersion-compensating fibers [2].

2.2 Fiber Bragg gratings

Fiber Bragg Grating is made of a periodic or slightly aperiodic modulation of the refractive index in the core of a single-mode fiber (fig. 3). Light guided along the structure will be scattered by each grating plane. The interference of fractional waves provides the back reflection at Bragg wavelength

$$\lambda_B = 2n_{eff}\Lambda \tag{2.24}$$

where n_{eff} is the modal index and Λ is the grating period. Partial reflections from each grating plane are in phase at λ_B. If the Bragg condition is not satisfied, the reflected waves from the subsequent planes become progressively out of phase and will eventually decay. When the Bragg condition is satisfied, the contributions of the reflected light from each grating plane will be added in the back-ward direction. This forms back-reflected peak in reflection with the center wavelength λ_B.

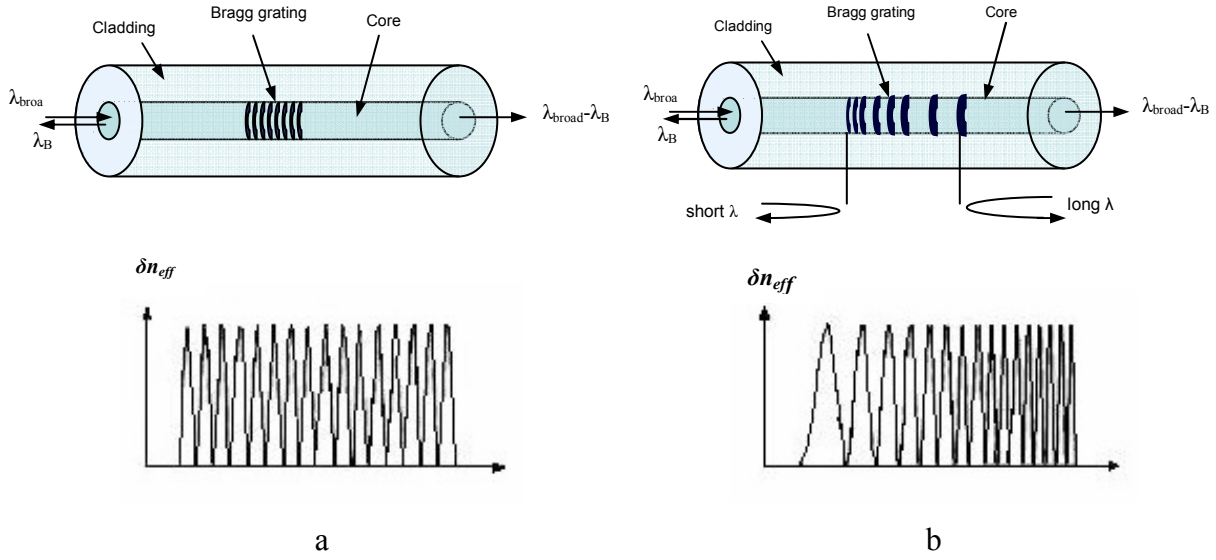

Fig. 3. Periodic (a) and aperiodic (b) refractive index modulation.

Any changes in the fiber properties, e.g. strain, temperature or polarization which varies the modal index and grating pitch, will shift the Bragg wavelength λ_B. This effect is widely used in application such as strain or temperature sensors [5], mode and polarization convectors [6, 7].

2.2.1 Fiber Bragg grating (FBG) characteristics

The Bragg condition obviously satisfies both the energy and momentum conservations. Energy conservation $\left(\hbar\omega_f = \hbar\omega_i\right)$ requires the identical frequency for the incident and reflected radiations. Momentum conservation requires that incident wave vector $\boldsymbol{k}_i$ plus the grating vector $\boldsymbol{K}$ is equal to the wave vector of scattered radiation $\boldsymbol{k}_f$, i.e.

$$\boldsymbol{k}_i + \boldsymbol{K} = \boldsymbol{k}_f , \tag{2.25}$$

where the grating wave vector $\boldsymbol{K}$ has a direction normal to the grating planes and has a magnitude of $2\pi/\Lambda$. The diffracted wave vector is equal in magnitude but opposite in direction to the incident wave vector. Thus, momentum conservation condition takes form of

$$2\left(\frac{2\pi n_{eff}}{\lambda_B}\right)=\frac{2\pi}{\Lambda}, \tag{2.26}$$

for the first-order Bragg condition given in Eq. (2.24) [5, 6].

The index perturbation in the core is a periodic structure, similar to a volume hologram or crystal lattice, forming a stop-band filter in which the incident optical field is reflected by successive, coherent scattering from the index variations [7].

According to coupled-mode theory [8], the index perturbation $\delta n(z)$ presented as a phase and amplitude-modulated periodic waveform

$$\delta n(z)=\delta n_0(z)\left[1+m\cdot\cos\left(\frac{2\pi z}{\Lambda}+\phi\right)\right]. \tag{2.27}$$

The average refractive index, the envelope of the index modulation and consequently the modal index n_{eff}, vary along the grating length. The contrast is given by parameter m that depends on the visibility of ultraviolet (UV) fringe pattern used for grating inscription.

The local reflectivity $r(z)$ is the complex ratio of the forward and backward propagating wave amplitudes. It is related to $\rho(z)$ by multiplicative phase factor $e^{-j\varphi}$. The modified reflectivity satisfies an equation

$$\rho'=j\left[\left(4\pi/\lambda_B\right)\left(\delta n_{eff}-\left(\delta\lambda/\lambda_B\right)-\phi'\right)\right]\rho+j\kappa(1+\rho^2) \tag{2.28}$$

with the boundary condition $\rho\left(L/2\right)=0$. The coupling coefficient κ is given by

$$\kappa=\left(\pi/\lambda\right)\delta n g(z)\eta, \tag{2.29}$$

where $g(z)$ is an apodization function, typically Gaussian or raised-cosine weighting, and η is a modal overlap factor. If the grating has low reflectivity, the Eq. (2.28) can be linearized and the reflectivity spectrum $\rho(-L/2, \delta\lambda)$ is proportional to the Fourier transform of $g(z)e^{-j\phi(z)}$. It is convenient to use this relationship for choosing amplitude weighting for a given filter characteristic. The reflectivity at line center $(\delta\lambda = 0)$ is

$$R = \rho\rho^* = \tanh^2\left[(\pi/\lambda)\delta n L \bar{g}\eta\right], \tag{2.30}$$

obtained by neglecting the chirp $\delta n_{eff}(z)$. This modeling approach provides an accurate prediction of the reflectivity and the grating spectrum.

In strongly reflecting gratings with large index perturbations, there are small sharp spectral resonances at the short wavelength edge of the grating spectrum. This effect can be explained using phase-matching condition [7].

$$n_{eff} - \frac{\lambda}{\Lambda_z} = n'_{eff}, \tag{2.31}$$

where n_{eff} is the modal index of the incident wave and n'_{eff} is the modal index of the grating-coupled reflected (a negative quantity) or transmitted wave. Graphical presentation of this condition is shown in Fig. 4.

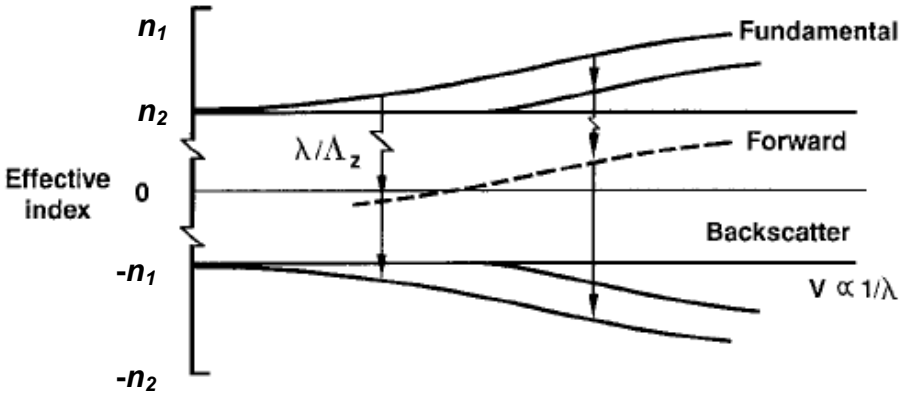

Fig. 4. Phase-matching conditions for synchronous mode coupling.

Ordinary-bound propagation occurs when the effective index of the wave ranges between the cladding and core index values with a grating pitch satisfying to the Bragg condition Eq. (2.24). When the effective index is less than the cladding index n_2, the cladding modes are not excited in the single-mode fiber. For opposite case, series of transmission dips in the spectrum appear at wavelengths shorter than Bragg wavelength (Fig. 5).

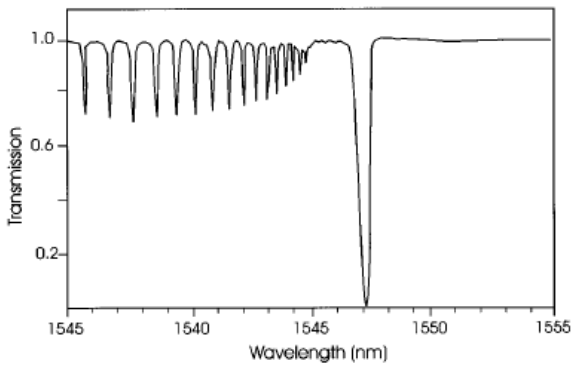

Fig. 5. Transmission spectrum of a grating in a single-mode fiber with cladding-mode lines.

2.2.2 Photosensitivity in optical fibers

Photosensitivity means that the index of refraction of the fiber changes under light exposure. It was demonstrated by Hill and co-workers in 1978 [9]. They irradiated the germanium-doped fiber with visible light (488 nm) from an argon ion laser. An increase in attenuation of the fiber has been observed. It was found that the intensity of the light back reflected from the fiber increases with the exposure time. It was also pointed out that the photosensitivity increases with the Ge dopant concentrations.

In 1989 Meltz et al [10] have shown that the index of refraction changes when germanium-doped fiber was exposed to UV light close to the absorption peak of a germanium-related defect at wavelength range of 240-250 nm. Later on the different models were proposed to describe the effect of the refraction index increase, based on color center, dipole [11], compaction and stress-relief mechanisms [6]. All these theories, however, assume that the germanium-oxygen vacancy defects, Ge-Si or Ge-Ge (the so-called “wrong bonds”) are responsible for the photoinduced index change.

During the high-temperature gas-phase oxidation process of the modified chemical vapor deposition (MCVD) technique, GeO_2 dissociates to GeO due to its higher stability at elevated temperatures. This species, when incorporated into the glass, can manifest in the form of oxygen vacancy Ge–Si and Ge–Ge ‘‘wrong bonds’’ responsible for photosensitivity

of highly doped germanosilica core optical fibers to UV radiation in the range of 240 – 250 nm. These oxygen vacancy defects have been directly linked to the mechanism of photoinduced refractive-index changes in the proposed models [6].

Photosensitive phenomena was found also in fibers doped with europium [12], cerium [13] and erbium:germanium [14].

Since the discovery of photosensitivity and the first demonstration of grating formation in germanosilica fiber, there were many efforts to enhance it. Particularly, boron codoping and hydrogen loading have been widely used for enhancing the photosensitivity of germanosilica fibers.

Boron codoping

Co-doping was found to increase dramatically the photosensitive response. The index modulation could reach values up to $\Delta n \sim 10^{-3}$ [15], which is much lager than value of $\Delta n \sim 10^{-5}$ achievable with ordinary single-mode fiber and $\Delta n \sim 10^{-4}$ for typical highly doped Ge-doped fiber. Now it is still not very clear why boron increases photosensitivity. There is assumption [16] that the addition of boron to the core of the fiber enhances the densification and stress relaxation after UV exposure, both contributed to the photoinduced refractive index change. Through germanium in B/Ge codoped fiber should be at the level of highly Ge-doped fiber without boron since boron decreases the refractive index. In the deposition process, proper flow of BCl_3 ensures the refractive index profile to be comparable to standard single-mode fiber (SMF).

Hydrogen loading of optical fibers

The highest increase in photosensitivity has been observed with hydrogen loading. Now it is practical technique for achieving high UV photosensitivity in germanosilica optical fibers. Hydrogen loading is carried out by diffusing hydrogen molecules into the fiber core at high pressure and temperature. This technique allows for large permanent change of the core refractive index. Index modulation of 10^{-2} can be achieved in standard fibers after UV exposure [17].

The diffusion of molecular hydrogen is described by diffusion equation

$$\frac{\partial C}{\partial t} - D\nabla^2 C = 0 \tag{2.32}$$

where C is the hydrogen concentration, and D is diffusion coefficient. According to Arrhenius-type relationship, the temperature dependence of the diffusivity is

$$D = D_0 \exp(\frac{-E_d}{kT}), \tag{2.33}$$

where D_0 is frequency factor, E_d is the activation energy, T is temperature in Kelvin and k is Boltzmann's constant. The diffusion coefficient for hydrogen in a fused silica is expressed as [18]

$$D = 2.83 \times 10^{-4} \exp\left(-\frac{40.19(kJ/mol)}{RT}\right) \tag{2.34}$$

where $R = 8.31 J/(K \cdot mol)$ is the gas constant.

The high concentration of hydrogen leads to high level of high power absorption and there is a large amount of losses. Hence the loaded fiber can not be used at once in communication system and it must be annealed. The solution for radial outward diffusion in cylindrical geometry is given by

$$\frac{C}{C_0} = 1 - \exp\left(-\frac{a^2}{4Dt}\right), \tag{2.35}$$

where a is the radius of the optical fiber, and t is the time after onset of diffusion for loaded sample.

The minimum annealing time in hours required to drive out 95% of hydrogen can be estimated as [19]

$$t(h) = 2.063 \times 10^{-4} \exp\left(\frac{4079}{T(K)}\right). \tag{2.36}$$

For annealing time longer that this, the hydrogen is nearly all driven out by diffusion from the fiber.

Above discussion is valid for steady-state process. The transient process is quite complicated and varies considerably for different types of silica. The reason for the complication is that chemical reactions of hydrogen with silica occur at the defect sites of the glass, and these defects vary considerably for various fibers. The chemical reaction can result in the formation of bound hydrogen, mostly in the form of hydroxyl [17, 18, 20].

2.2.3 Uniform Bragg gratings

Uniform fiber Bragg grating consists of a periodic modulation of the index of refraction in the core of a single-mode fiber (fig. 6). The refractive index profile estimated by (2.27) satisfies the Bragg condition (2.24).

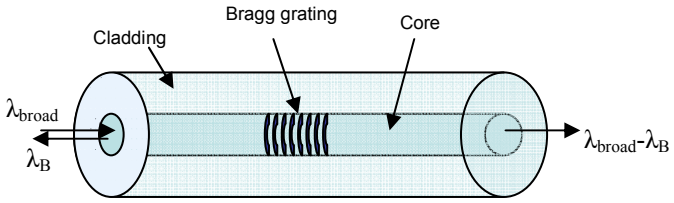

Fig. 6. Illustration of a uniform Bragg grating.

Using the coupled-mode theory analytical description, the reflection properties of Bragg grating can be obtained. The reflection of uniform grating is given by [21]

$$R(L,\lambda) = \frac{\Omega^2 \sinh^2(sL)}{\Delta k^2 \sinh^2(sL) + s^2 \cosh^2(sL)}. \tag{2.37}$$

$R(L,\lambda)$ is a function of grating length L and wavelength λ. Ω is coupling coefficient, $\Delta k = \beta - \pi/\Lambda$ is detuning wave vector, β is propagation constant and $s = \sqrt{\Omega^2 - \Delta k^2}$. The coupling coefficient Ω for the sinusoidal refractive index modulation can be introduced as

$$\Omega = \frac{\pi \delta n \eta(V)}{\lambda} \tag{2.38}$$

where $\eta(V)$ is function of fiber V equal approximately to $\eta(V) = 1 - 1/V^2$. A calculated reflection spectrum as a function of the wavelength is shown in Fig. 7. The side lobes are due to multiple reflections to and from opposite ends of the grating region.

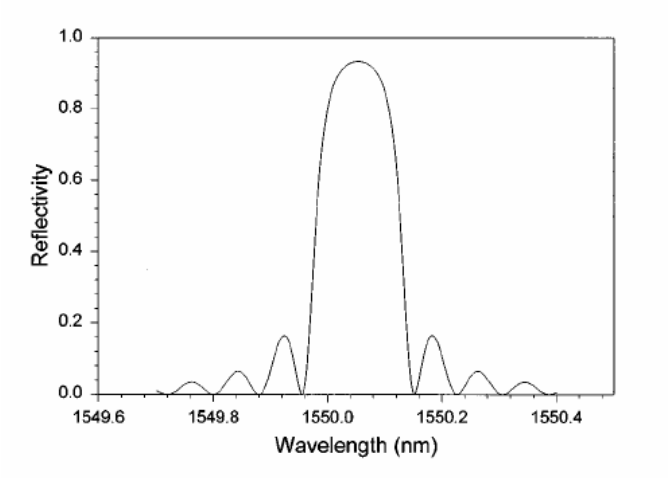

Fig. 7. Bragg grating reflection spectrum.

At the Bragg resonant wavelength there is no wave vector detuning, $\Delta k = 0$ and the reflectivity becomes

$$R(L, \lambda) = \tanh^2(\Omega L). \tag{2.39}$$

The reflectivity increases as the induced refractive index of refraction change increases.

A general equation for the approximate full width at half-maximum bandwidth of a grating is given by

$$\Delta\lambda = \lambda_B \alpha \sqrt{\left(\frac{\Delta n}{2n_0}\right)^2 + \left(\frac{1}{N}\right)^2}, \tag{2.40}$$

where N is number of the grating planes. The parameter α is ~ 1 for strong gratings with near 100% reflection, whereas $\alpha \sim 0.5$ for weak gratings [6].

When the grating is formed with a saturated exposure, then the effective length will be reduced as the transmitted signal depleted reflection. As a consequence, the spectrum will broaden considerably and depart from a symmetric sinc or Gaussian-shape spectrum whose width is inversely proportional to the grating length (Fig. 8) [7].

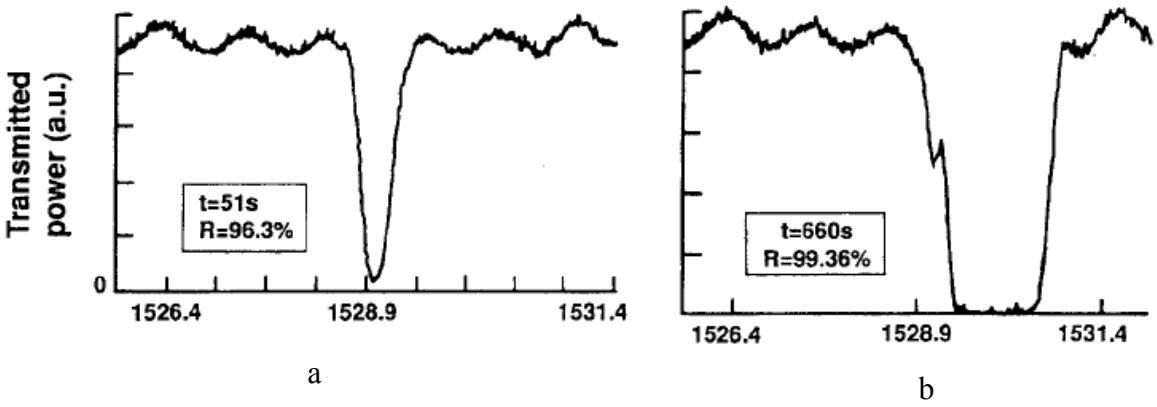

Fig. 8. Bragg grating with a large index change becomes saturated (a) and after long exposure (b).

Uniform fiber gratings are widely used in various devices in fiber optics. Particularly, they are employed as spectrally selective elements in fiberoptics communication systems [1], in various types of fiber lasers and amplifiers [22], and in different kinds of the sensor applications [23, 4].

2.2.4 Linearly chirped Bragg gratings

Chirped Bragg grating is a grating with a variable grating period (fig. 9). It can be realized by two methods (see Eq. 2.24): one is to change the pitch period, another is to change an effective refractive index along the propagation direction in the fiber.

The refractive index of the chirped Bragg grating according to the coupled-mode theory can be expressed by [24]:

$$n(x,y,z) = \vec{n}(x,y,z) + \delta n(x,y,z)\cos\left(\frac{2\pi z}{\Lambda} + 2\int_0^z \phi(\xi)d(\xi)\right), \qquad (2.41)$$

where Λ is the grating period, and $\phi(\xi)$ describes the local phase of the chirped grating.

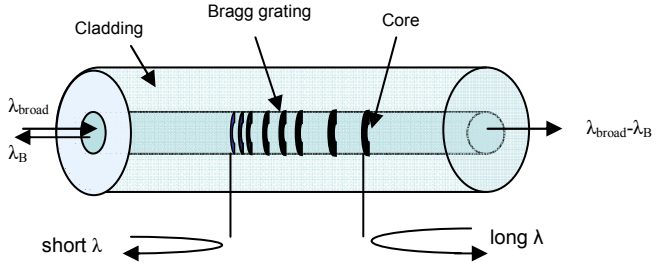

Fig. 9. Linearly chirped fiber Bragg grating.

When the period changes along the z-direction, the Bragg wavelength λ_B becomes dependent on the location. Changing an effective refractive index n_{eff} along z-direction has the similar effect as changing the period along the z-direction. This means that the optical period could be changed even when the physical period of the grating is fixed.

The phase slope for linearly chirped grating is given by [24]

$$\frac{1}{2}\frac{d\phi}{dz} = -\frac{4\pi n_{eff} z}{\lambda_B^2}\frac{d\lambda_B}{dz}, \tag{2.42}$$

where $d\lambda_B / dz$ is a rate of change of the Bragg wavelength with position in a fiber. For the linearly chirped grating, the chirp variable $d\lambda_B / dz$ is constant which means that the period of the grating varies linearly with position. As a consequence, a chirped Bragg grating introduces different temporal delays for different wavelengths. The dispersion of the grating in reflection for the spectral component corresponding to edges of the grating spectral bandwidth is equal to twice the propagation delay through the grating [6]

$$\tau = \frac{2L}{v_g}, \tag{2.43}$$

where L is grating length and v_g is the group velocity of the pulse incident on the grating. Therefore, a grating with a linear wavelength chirp of $\Delta\lambda$ nm will have a dispersion of [6]

$$D = \frac{\tau}{\Delta\lambda} \text{(ps/nm)}. \tag{2.44}$$

The wavelength dependent temporal delay is commonly used for dispersion compensation [25, 26, 27]. The chromatic dispersion of the fiber creating larger delay for the lower-frequency components can be compensated using chirped fiber grating producing lager delay for the higher-frequency components.

Also chirped fiber Bragg grating could be used as integrating sensor of temperature [28] and strain [29].

2.2.5 Strain and temperature sensitivity of Bragg gratings

Bragg grating wavelength depends on the effective index of refraction of the core and the periodicity of the grating. It can be used to monitor the changes in strain and temperature. Using Eq. (2.24), the shift in the Bragg grating centre wavelength due to strain and temperature changes can be written as [6]

$$\Delta\lambda_B = 2\left(\Lambda\frac{\partial n}{\partial l} + n\frac{\partial\Lambda}{\partial l}\right)\Delta l + 2\left(\Lambda\frac{\partial n}{\partial T} + n\frac{\partial\Lambda}{\partial T}\right)\Delta T\,. \tag{2.45}$$

The first term represents the strain induced effect in an optical fiber. The wavelength shift $\Delta\lambda_B$ for an applied longitudinal strain $\Delta\varepsilon$ can be expressed as

$$\Delta\lambda_B = \lambda_B(1-\rho_\alpha)\Delta\varepsilon\,, \tag{2.46}$$

where ρ_α is the photoelastic coefficient of the fiber, given by

$$\rho_\alpha = \frac{n^2}{2}[\rho_{12} - \nu(\rho_{11} - \rho_{12})], \tag{2.47}$$

where ρ_{11} and ρ_{12} are the components of the fiber-optic strain tensor and ν is Poisson's ratio.

The chirped Bragg gratings for strain sensors use the effective change in reflection location δb which is given by

$$\delta b = -\frac{\lambda}{\Delta\lambda_C}B\varsigma\Delta\varepsilon \tag{2.48}$$

where ς is constant determined by the photoelastic properties of the fiber and B is the grating length. λ is a fixed source wavelength and $\Delta\lambda_C = \lambda_{B1} - \lambda_{B2}$ with $\lambda_{B1} < \lambda_{B2}$ (from fig. 10.). For comparison, the change of the optical length of the fiber with length of B is given by

$$\delta l = B\varsigma\Delta\varepsilon\,. \tag{2.49}$$

The ratio of equations (2.48) and (2.49) is expressed in the form

$$\frac{\delta b}{\delta l} = -\frac{\lambda}{\Delta\lambda_C}\,. \tag{2.50}$$

Since $\lambda >> \Delta\lambda_C$ and $\delta b >> \delta l$, chirped FBG gives a very large strain transduction amplification factor [4].

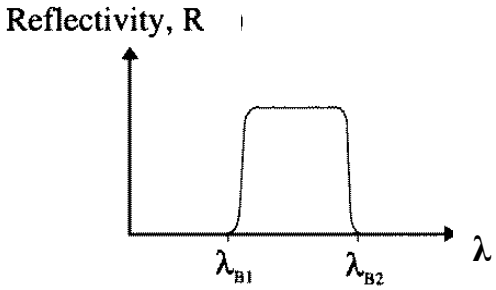

Fig. 10. Chirped fiber Bragg grating reflection spectrum.

The second term of Eq. (2.45) represents the temperature effect. For temperature change of ΔT, the corresponding wavelength shift $\Delta\lambda_{BT}$ is given by [4]

$$\Delta\lambda_{BT} = \lambda_B(\alpha + \xi)\Delta T\,, \tag{2.51}$$

where α is thermal expansion coefficient for fiber and ξ is the fiber thermo-optic coefficient. For pure silica, the thermal expansion coefficient is approximately $\alpha = 0.55\times10^{-6}\,(°\mathrm{C})^{-1}$ and the thermo-optic coefficient is $\xi = 6.7\times10^{-6}\,(°\mathrm{C})^{-1}$ [30].

3 FABRICATION TECHNOLOGY AND CHARACTERIZATION OF FIBER BRAGG GRATINGS

3.1 Workstation for fiber Bragg grating fabrication

Fiber Bragg gratings were made using phase-mask technique [31]. This method is based on the diffraction of UV light by a mask placed closely to the fiber.

The phase-mask technique is significantly simpler in comparison with other methods. It has simple setup and uses low coherence UV laser beam.

In my work I used KrF excimer laser COMPex by Lamda Physik GmbH. The operation principle is based on the chemical reaction between inert gas and halogen gas. It requires the elevation of the inert gas atom to its reactive exited state. The energy schematic and the laser transition of the "ionic channel" of the KrF excimer laser are shown in Fig. (11). Excitation of the active media of an excimer laser is performed by kinetic processes, involving a third body collision partner ("buffer gas"). The threefold collision of the Kr^+ and F^- ion and the collision partner results in the formation of the upper laser level (B state). Although the potential energy well of the excited molecule is deep, it is unstable and decays after less than 10ns to its ground state (X-state). This transition of the molecule corresponds to the laser radiation. After the decay of excited molecule, the components are available for a new excitation cycle [32].

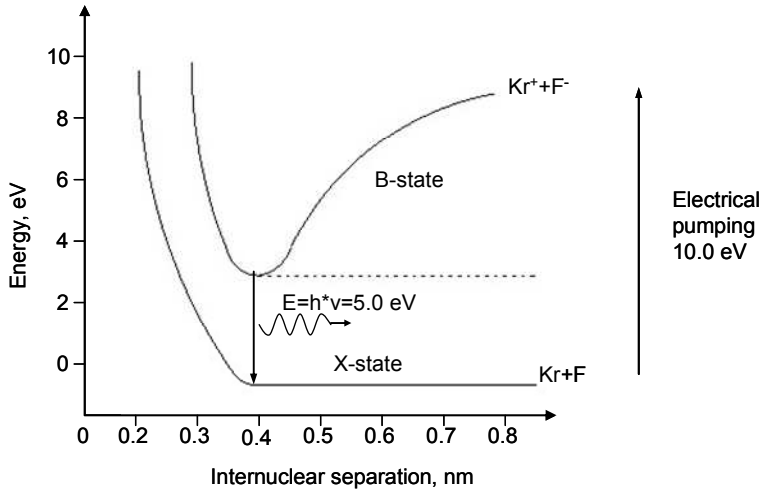

Fig. 11. Energy schematic diagram for the KrF excimer laser.

It is necessary to refill regularly the gas. The change of laser beam energy during the work period between refilling is presented in Fig. 12. Usually laser period is equal to one month when the system works normally. This dependence was made when the cooling system did not work resulting in reduced working time. The laser was also extensively employed during the work, resulting in faster degradation of the gases compared to usage several times in a week.

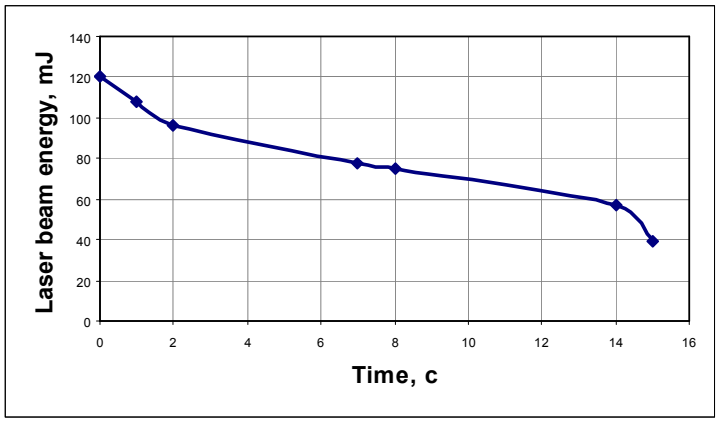

Fig. 12. Degradation of laser beam energy during the work period (U = 24kV).

The fiber Bragg grating manufacturing workstation developed by INESC Porto is shown at the Fig. (13). It consists of 4 sub-assemblies:

1. beam scan sub-assembly;
2. phase mask sub-assembly;
3. optical fiber sub-assembly;
4. machine-vision sub-assembly.

All sub-assemblies are situated on the vibration isolation platform, which provides ultra stability of the system. Controlling of the system realizes by LabVIEW program.

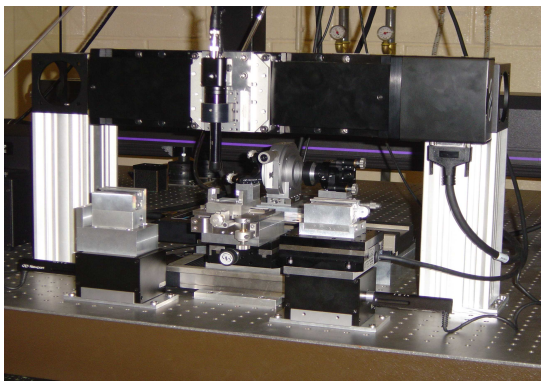

Fig. 13. Workstation for fabrication of fiber Bragg gratings.

The beam scanning assembly consists of a linear air-bearing scanning stage, cylindrical lens mount, and precision optical slit (Fig. 14). The scanning stage provides the means to perform multiple scans of the fiber during the writing operation. The beam can be scanned over a length from 0.0 mm to 100.0 mm, with a position resolution of 0.002 μm. The cylindrical lens mount can be moved in *x*-*y* plane and *z*-direction. The first one allows to provide adjustable orientation about the pitch and yaw axes and continuously rotation along the optical axis over 360°. The *z*-axis is adjustable to allow the focus change.

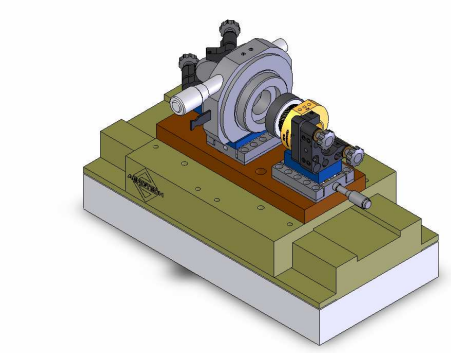

Fig. 14. Detail of the 3D CAD design view of beam scan sub-assembly.

Second sub-assembly is the phase mask support that provides means to reliably mount and position the phase mask (Fig. 15). The assembly includes a tilt platform to provide two-axis angular alignment of the phase mask with high precision, an ultra-compact size and high reliability motorized stage for phase mask to optical fiber positioning. The range of motion of this motorized stage is from -50.0 mm to +50.0 mm with the translation accuracy of ±1.5 μm.

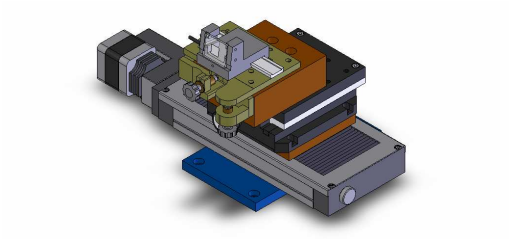

Fig. 15. Detail of the 3D CAD design view of phase mask sub-assembly.

One of the most important parts of the workstation is fiber handling sub-assembly (Fig. 16). The fiber handling sub-assembly provides capability to load and unload, to apply mechanical tension and to adjust the height position of the optical fiber. The strain mechanism provides a constant strain after the fiber is properly fixed prior to writing and positioning of the fiber and during the exposure process. The range of axial strain applied to the fiber is 0.1 N to 10 N, with reproducibility within ±0.05 N.

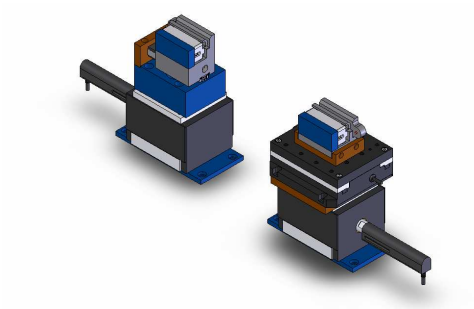

Fig. 16. Detail of the 3D CAD design view of optical fiber sub-assembly.

The last part of the workstation is the machine vision alignment system (fig. 17). It provides capability to control precisely position of the optical fiber with respect to the phase mask in a range from 10.0 µm to 300.0 µm. The system includes a high resolution camera equipped with a high magnification video lens and a structural rail gantry to support the camera translation stage.

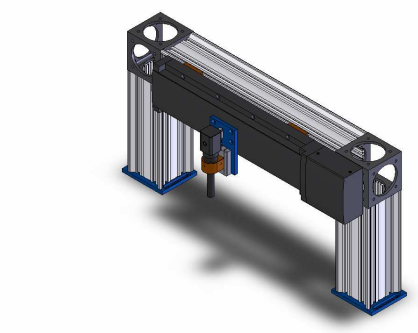

Fig. 17. Detail of the 3D CAD design view of machine-vision sub-assembly.

3.2 Manufacturing of the fiber Bragg gratings

In this work OFS single-mode fiber was used. Its properties are shown in table 1. This fiber is formally known as “980 Coupler Fiber” and widely used in many applications.

Table 1. OFS single-mode fiber properties.

Properties	**Value**
Operating wavelength	980/1550 nm
Cutoff wavelength	≤960 nm
Attenuation @ 980 nm	≤3.0 dB/km
Numerical aperture	0.16
Core diameter	4.4 μm
Clad diameter	125±2 μm
Coating diameter	245±2 μm
Coating material	Dual UV Acrylate
Operating temperature	- 40 to + 85°C

As it was mentioned earlier I used phase mask technique for fabricating the fiber Bragg gratings (Fig. 18). The phase mask consists of one-dimensional surface-relief structure fabricated in a high fused silica flat transparent to the KrF eximer laser radiation. The surface-relief structure is designed to suppress the zero-order diffracted beam down to 5 % and to maximize plus-one and minus-one orders (typically more than 35 %). When light of plus-one and minus-one order overlap, an interference pattern is produced. The period of this pattern is not a function of the inscribing wavelength. The interference pattern photoimprints a refractive-index modulation in the core of a photosensitive optical fiber. Where the intensity is high the index of refractivity is increasing.

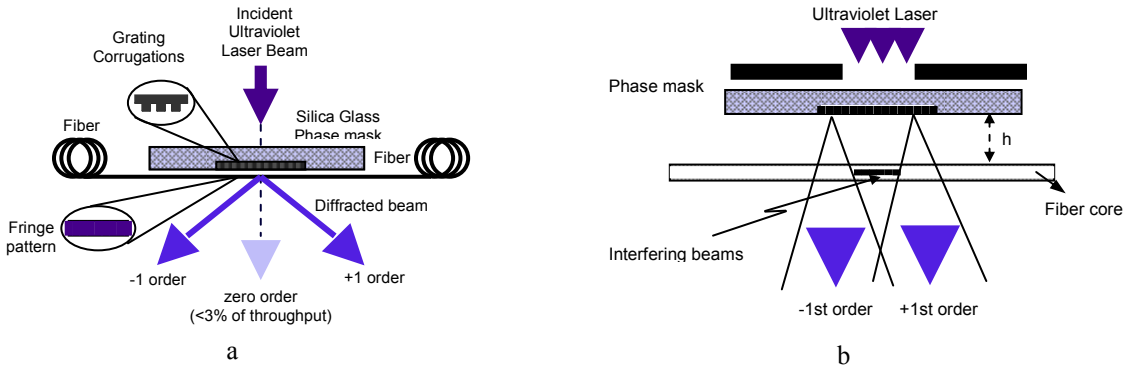

Fig. 18. Schematic of the phase-mask technique (a) and phase-mask geometry (b) for inscribing Bragg grating in optical fibers.

3.2.1 Uniform Bragg gratings

Uniform fiber Bragg grating is a grating with a periodic modulation of the refractive index (Fig. 3). The grating obeys the Bragg condition Eq. (2.24) corresponding to the reflection maximum at λ_B.

Prior grating inscription, the fiber is solidly fixed at the optical fiber sub-assembly (Fig. 16). Strain in amount of 1 N is typically applied to the fiber axis automatically using the computer program. Then the program executes aligning between phase mask and fiber. It is an important issue permitting to decrease losses and get high quality gratings. After the aligning is completed, the laser beam begins to expose the fiber through the mask without beam scanning. The slit in the beam scan sub-assembly (Fig. 14) was not used and the fiber was exposed to the whole beam.

The different kinds of phase masks were used to achieve the different λ_B. The parameters of these masks and the Bragg wavelengths are presented in the table 2. Note that the Bragg wavelengths pointed in the table are specific to the particular type of the fiber.

Table 2. The parameters of the uniform phase masks and corresponding Bragg wavelengths.

№	Supplier	Pitch, nm	Inscription wavelength, nm	λ_B, nm
1	Stocker Yale	714.99	248	1039.404
2	Stocker Yale	730.69	248	1061.928
3	Ibsen	744.51	248	1081.936

The transmission and reflection spectra of different manufactured uniform fiber Bragg gratings are shown in the Ffig. 19.

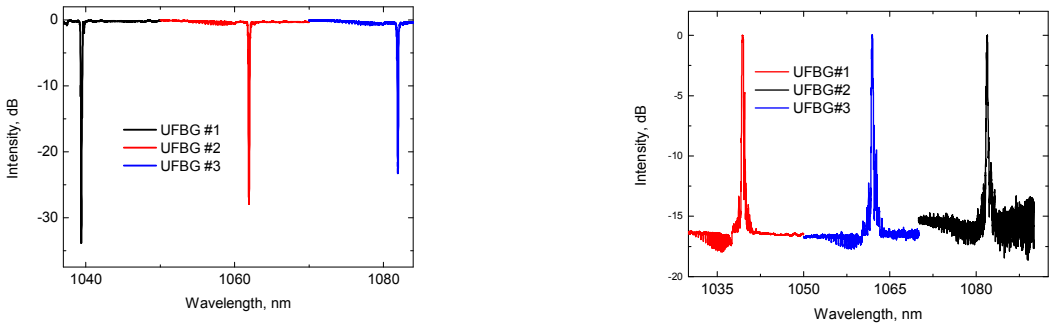

a b

Fig. 19. Uniform fiber Bragg gratings with different Bragg wavelengths: ttransmission spectrum (a) and reflection spectrum (b).

3.2.2 Chirped Bragg gratings

Chirped Bragg grating was a grating with a variable grating period (Fig. 9). It can be realized by changing the Bragg period or changing the refractive index along the grating. In my work I used the first method for fabricating chirped Bragg grating. It was realized by chirped phase masks. The period of the phase mask grating varies linearly along the grating. The parameters of the phase mask used in the fabricating process are shown in the table 3.

Table 3. The parameters of the phase masks used for fabrication of chirped fiber Bragg gratings.

№	Supplier	Pitch, nm	Chirp, nm/cm	Inscription wavelength, nm
1	Stocker Yale	715.01	15	248
2	Ibsen	715.00	7	244
3	Ibsen	715.00	1.4	248

The reflection spectra of different manufactured chirped fiber Bragg gratings are presented in the Fig. 20.

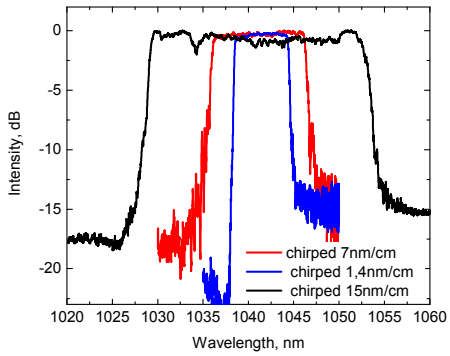

Fig. 20. The reflection spectra of the chirped fiber Bragg gratings.

The strain applied along the fixed fiber was equal to 1 N. Then the relative position of the phase mask and the fiber is adjusted using machine-vision sub-assembly (Fig. 17) and the program control. In this case it is important to use scanning system to get high quality grating. The rate of the scanning is usually of 0.0025 mm/s.

The chirped fiber Bragg grating has feature that the reflection spectrum when illuminated from one side (short wavelength side) is not identical to the spectrum when illuminated from the opposite side (long wavelength side) (Fig. 21). This asymmetry is utilized in dispersion compensators for high-speed communication. The reason of this phenomenon is a different chirp for counter coming lights. Besides this the reflection light for long wavelength side contains the cladding losses which appear mainly due to grating tilt [33].

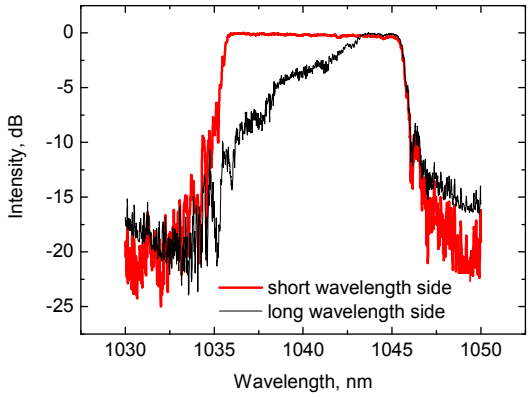

Fig. 21. The reflection spectra of the chirped fiber Bragg grating from short and long wavelength sides.

The cladding mode losses can be decreased by avoiding the phase mask tilt relative to the fiber axis.

3.3 Characterization of Bragg gratings through transmission and reflection measurements

For characterization of fiber Bragg grating the transmission and reflection measurements were performed using broadband (white light) source, as shown in the Fig. 22. This system consists of 980 nm pump laser, wavelength-division multiplexing coupler (WDM), Yb-doped fiber, optical isolator, fiber coupler 50/50 and spectrum analyzer.

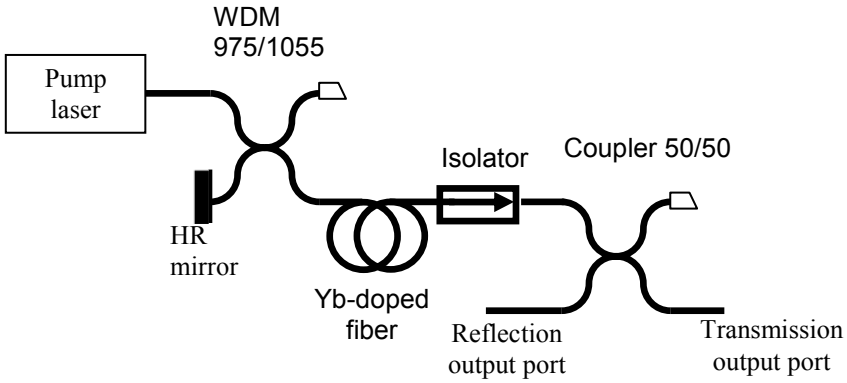

Fig. 22. The scheme of the system for fiber Bragg grating characterization.

High-power 980 nm fiber-coupled laser module developed by Bookham was used as a pump source for erbium and ytterbium doped fiber amplified spontaneous emission (ASE) device. The laser diode delivers kink free output powers up to 750 mW. The laser center wavelength is 974.2 nm and has narrow band spectrum. Broad band spectrum of Yb-fiber ASE source is shown in Fig. 23.

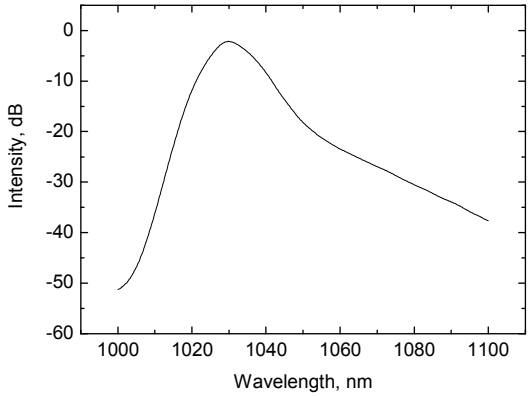

Fig. 23. The ASE source spectrum.

Wavelength-division multiplexing is used to multiplex in a fiber two optical signals with different wavelengths, i.e. pump and ASE emission. In this system 975/1055 WDM made at ORC is used to combine 975 and 1055 nm wavelengths.

Since the fiber Bragg grating reflects back the light, it is necessary to protect broadband source from the back signal. For this case the polarization insensitive isolator is used for white-light measurements system.

The coupler 50/50 splits the optical power in proportional 50% to 50% that allows to measure transmission and reflection spectrum from the appropriate output ports.

3.4 Hydrogen loading of the fibers: technique and chamber description

The procedure of hydrogen loading is used for enhancement of fiber photosensitivity as it was mentioned in the subchapter 2.2.2. Hydrogen loading was realized in the chamber, shown in Fig. 24. Under pressure of 140 bar and elevated temperature, hydrogen diffuses efficiently into the fiber during a time of few days.

Fig. 24. Photograph of hydrogen loading chamber.

The aim of the measurements was to determine the minimum loading time that ensures sufficient photosensitivity. The criterion of the loading effect was the time required to inscript FBG with the reflectivity more than 95 %. For getting this estimation the optical fibers were in the chamber during 17 hours, 1, 2, 3, 4, 5, and 6 days and then the

transmission spectrum was measured (Fig. 25). The given value of the reflectivity has been achieved for the fiber with the loading time above 3 days.

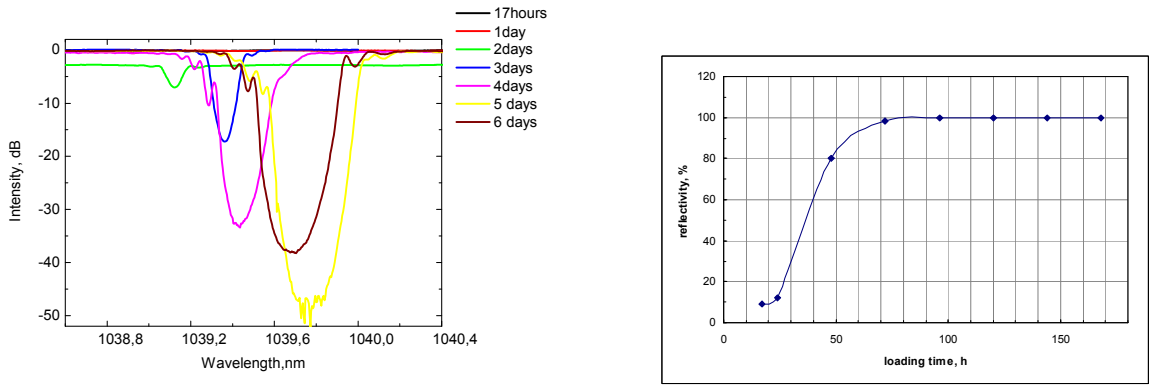

a b

Fig. 25. The transmission spectrum of uniform fiber Bragg gratings with different loading times (a); dependence of reflectivity on loading time (b).

For the chirped fiber Bragg grating, however, 3 days of the loading period is not sufficient to get high quality grating, as it was found from experiments. The reflection spectra of the CFBG with chirp of 7 nm/cm depending on the loading time are presented in Fig. 26. As seen in Fig. 26, smooth reflection response of a CFBG with a chirp rate of 7 nm/cm is achieved with a minimum hydrogen loading time of 7 days. Also it was found out that the larger values of chirp need more pulse energy for the inscription.

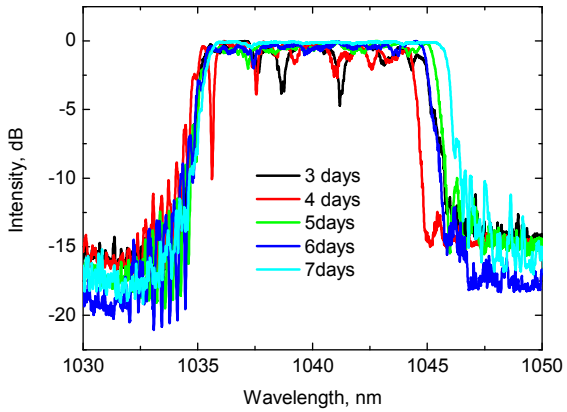

Fig. 26. The reflection spectra of the CFBG for different loading times.

3.5 Hydrogen removal by annealing

However, after the fabrication, the fiber Bragg gratings can not be used in optical system immediately because of high hydrogen concentration in a fiber resulted in an increased loss and prevented high-quality splicing. Hence annealing of the hydrogen is a necessary procedure. However, this process may decrease of the gratings reflectivity and result in wavelength shift of the UFBG.

In this work hydrogen annealing was carried at the two different temperature conditions: at the room temperature and in the oven at 72 - 75°C. There is no big difference in changes of grating parameters consequently of annealing process at different temperatures except of time. Theoretical calculations of the minimum annealing time can be estimated by Eq. (2.36). For 95% loaded fiber which is annealed at room temperature the minimum annealing time is equal to 199 hours (see attachment), and at 75°C it is equal to 25 hours.

3.5.1 Hydrogen induced losses vs. annealing time

Absorption of hydrogen molecules was observed to be decreased progressively during hydrogen out diffusion. The loss measurements were provided with 1.77 m long OFS fiber. The scheme of the measurements is presented in Fig. 27.

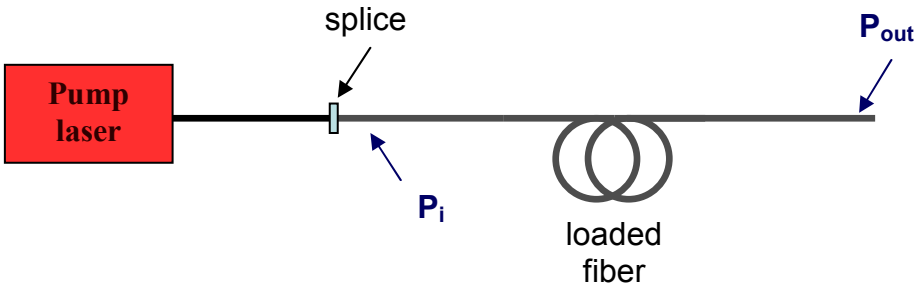

Fig. 27. The scheme of the loss measurement setup.

The estimation of attenuation was made according to the equation

$$\alpha(dB/m) = -\frac{10}{L}\log_{10}\left(\frac{P_{out}}{P_{in}}\right) \tag{3.1}$$

where α is attenuation coefficient, P_{in} is power launched at the input end of a fiber with length L and P_{out} is output power. The results of the measurements are presented in Fig. 28. After annealing, when the nearly all hydrogen has been removed out from the fiber, the level of attenuation decreased by 6 times.

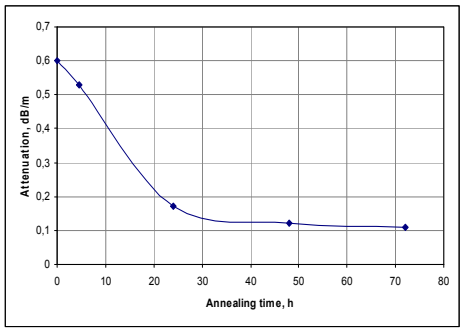

Fig. 28. The change in the attenuation of optical fiber during annealing time.

Note that the value of splice losses varied from 45% at the beginning of the annealing process to approximately 0% at the end.

3.5.2 Decrease in the reflectivity caused by the annealing

During the annealing decrease in reflectivity was observed due to decrease in effective refractive index. The decay of gratings reflectivity is shown in Fig. 29.

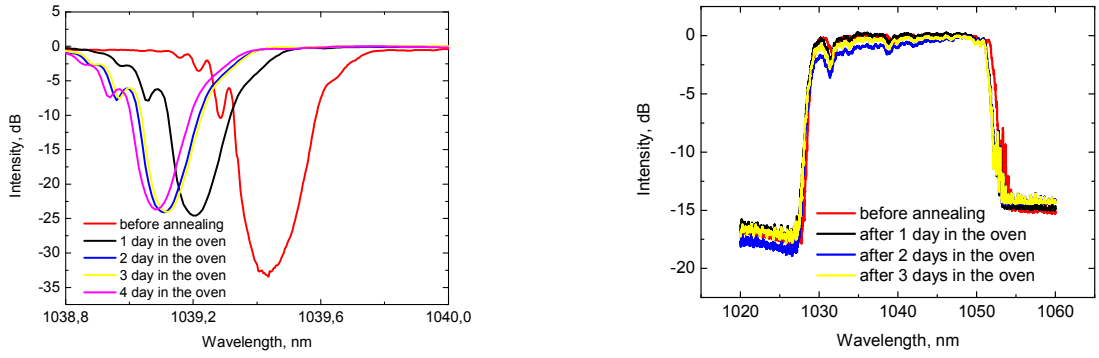

a b

Fig. 29. Change in reflection spectra of UFBG (a) and CFBG during annealing in the oven (b).

As it can be seen from Fig. 29 the changes in reflectivity are not high. The difference between reflectivity before annealing process and after is equal to 0.1%.

3.5.3 Wavelength evolution of FBG during annealing

The annealing causes also the Bragg wavelength shift as it can be seen from Fig. 30. The reason of this phenomenon is gradual hydrogen out-diffusion. First, the hydrogen diffuses out preferably from the cladding resulting in the decrease of the refractive index. Hence the difference between the refractive index of the cladding and core increases causing the wavelength shift to the larger values. Then the out-diffusion from the core leads to equalizing of the refractive index difference and, consequently, the wavelength shifts to the lower values.

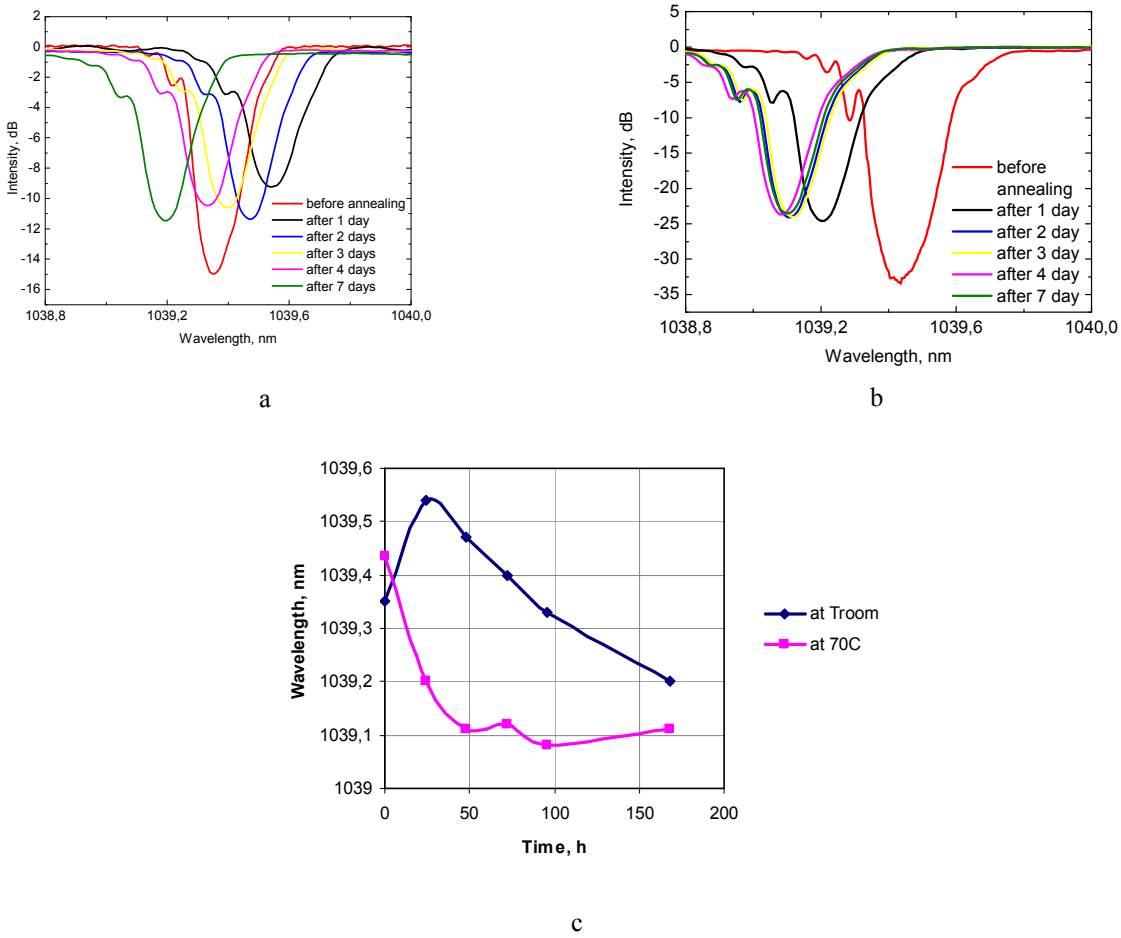

Fig. 30. The wavelength evaluation of UFBG during annealing process: transmission spectra of UFBG for different annealing times at room temperature (a); transmission spectra of UFBG for different annealing times at 70°C (b); wavelength evolution at room temperature and 70°C (c).

This effect can be easy observed when the annealing process occurs at room temperature because of lower annealing rate ($D = 2.269\times10^{-11}$). When the out-diffusion takes place at higher temperature ($D = 2.607\times10^{-10}$), the wavelength shift to the larger values and back happens during 2-3 hours after the beginning of the process. The time needed to completely

stabilize the Bragg wavelength is approximately 7 days for room temperature annealing and 2 days for 70°C.

4 APPLICATIONS: STRAIN AND TEMPERATURE SENSORS USING FIBER BRAGG GRATINGS

Effective index of refraction of the fiber core is strongly affected by external perturbations, and because of the changes in effective index cause changes in Bragg wavelength. In this chapter I describe the experimental dependences of UFBG and CFBG Bragg wavelengths on the strain and temperature.

4.1 Strain sensor

By applying longitudinal tension to the grating, the Bragg wavelength shift that occurs is proportional to the value of the tension according to Eq. (2.46). The measurements of this dependence were made for three UFBG with different Bragg wavelengths shown in table 2 and for two CFBGs with chirps of 7 nm/cm and 1.4 nm/cm. The tension was applied using the fiber handling sub-assembly (Fig.16) and computer control. The tension range varied from 0.1 to 3 or 5 N until the FBG was damaged.

The wavelength shifts for UFBG are presented in Fig. 31. The slope of the wavelength shift was nearly similar for all studied UFBG, as seen from Fig. 31 b. The strain sensitivity coefficients of the gratings are equal to 1.0723 nm/N (UFBG#1), 0.8277 nm/N (UFBG#2) and 0.8733 nm/N (UFBG#3).

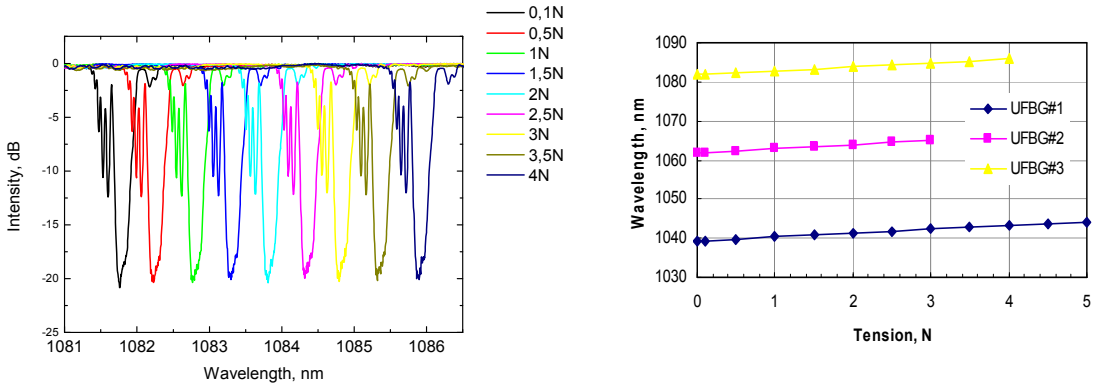

a b

Fig. 31. Transmission spectra of UFBG for different tensions (a); wavelength shifts versus applied tension for different kinds of UFBG (b).

The change in the CFBG spectrum is shown in Fig. 32. The rate of wavelength shift is approximately the same for 7 nm/cm and 1.4 nm/cm chirp gratings, as can be seen from Fig. 32 b.

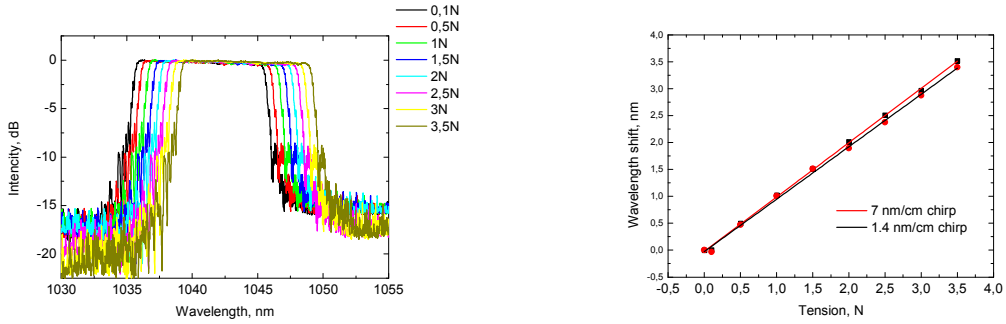

a b

Fig. 32. Reflection spectra of GFBG for different tensions (a); wavelength shifts versus applied tension for different CFBG (b).

4.2 Temperature sensor

The temperature measurements were made using the oven shown at the Fig. 33. The gratings were fixed inside the oven and the spectra were measured from appropriate output ports (transmission for UFBG or reflection for CFBG). The oven rises up the temperature linearly with the accuracy of 0.1°C. The temperature range used in these measurements varied from 20 to 130°C. The measurements were performed for both UFBG and CFBG.

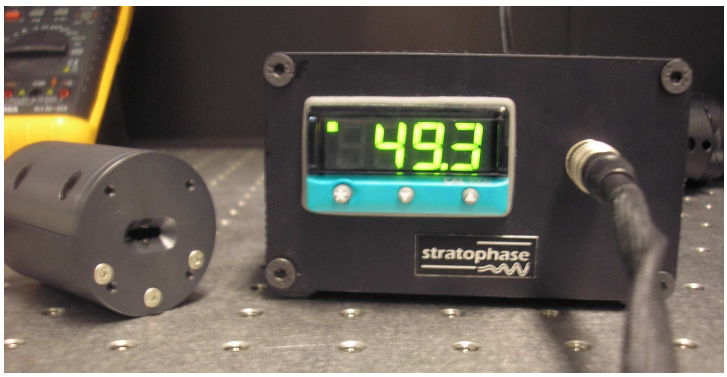

Fig. 33. The oven used for temperature sensor measurements.

The Bragg wavelength shifts for UFBG #2 and #3 are shown in Fig. 34. The temperature slope coefficient is equal to 0.007 nm/°C for both UFBG #2 and #3.

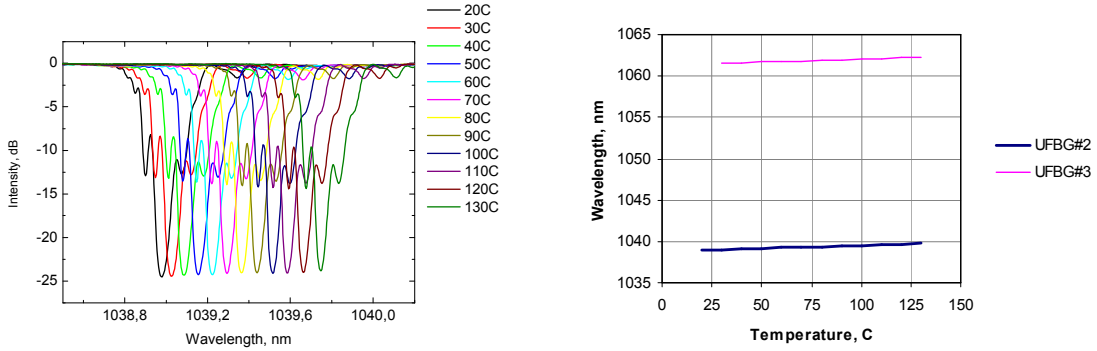

a b

Fig. 34. Transmission spectra of UFBG for different temperatures (a); wavelength shifts versus temperature for different UFBG (b).

The wavelength shift of GFBG due to ambient temperature variation is presented in Fig. 35. The temperature slope coefficients are equal to 0.006 nm/°C and 0.007 nm/°C for 7 nm/cm and 1.4 nm/cm chirp gratings, respectively.

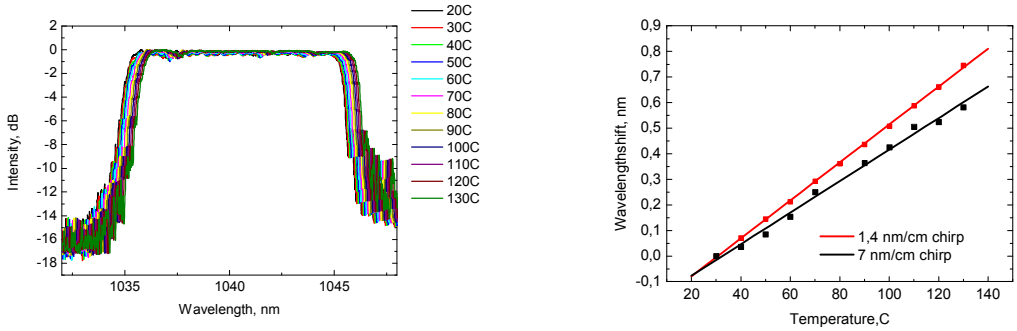

a b

Fig. 35. Reflection spectrum of GFBG for different temperatures (a); wavelength shift versus temperature for different CFBGs (b).

Note that tension changes influence for the wavelength shift more than temperature changes either for UFBG or for CFBG.

5 CONCLUSIONS

In this thesis the fabrication technology of UFBG and CFBG has been studied. Various kinds of gratings were made by phase mask technique using UV excimer laser. The characterization of FBG was performed by recording the transmission and reflection spectra obtained with broadband light source.

The main focus of this study was a hydrogen loading technique. The optimal loading condition has been determined. 3 days for UFBG and 7 days for CFBG at T=50°C and hydrogen pressure of 140 bar was found to be an optimal regime that ensures sufficient photosensitivity of the fiber. The post-inscription annealing is required to suppress excess losses induced by the hydrogene. High concentration of hydrogen also affected reflectivity and central wavelength of FBG. The efforts were made to minimize this effect. It was found out that the central wavelength of a grating was completey stabilized after two days annealing at 70 °C or 7 days at room temperature.

The FBG is widely used in different sensors. I have performed strain and temperature sensor measurements with UFBG and CFBG. Different tensions and temperatures were applied to the gratings causing wavelength shift which was measured. This kind of robust and cost-effective grating sensors can be used in various industrial and environmental applications.

ATTACHMENT

The diffusion coefficient for hydrogen in a fused silica (Eq. 2.34)

at T=23°C

$$D = 2.83 \times 10^{-4} \exp\left(- \frac{40.19 \times 10^{3} J / mol}{8.31 J /(K \cdot mol) \cdot 296 K} \right) = 2.269 \times 10^{-11} \text{ mol/h}$$

at T=75°C

$$D = 2.83 \times 10^{-4} \exp\left(- \frac{40.19 \times 10^{3} J / mol}{8.31 J /(K \cdot mol) \cdot 348 K} \right) = 2.607 \times 10^{-10} \text{ mol/h}$$

The calculation of the minimum annealing time required to drive out 95% of hydrogen (Eq. 2.36):

at T=23°C

$$t = 2.063 \times 10^{-4} \exp\left(\frac{4079 K}{296 K} \right) = 199 \text{ hours}$$

at T=75°C

$$t = 2.063 \times 10^{-4} \exp\left(\frac{4079 K}{348 K} \right) = 25.4 \text{ hours}$$

REFERENCES

1. G. P. Agrawal. Fiber-Optic Communication Systems. A John Wiley&Sons, Inc., Third Edition, 2002;
2. http://www.fiber-optics.info/articles/fiber-types.htm;
3. R. Ramaswani, K. N. Sivarajan. Optical Networks: A Practical Perspective. Morgan Kaufmann, San-Francisco, 1998;
4. Rao Y.-J. In-fibre Bragg grating sensors. Review article. Meas. Sci. Technol., vol.8, pp.355-375 (1997);
5. Yoon H.-J. et al. In situ strain and temperature monitoring of adaptive composite metrials. J. of Intelligent Material systems and Structures, vol. 17, pp.1059-1067 (2006);
6. Othonos A. Fiber Bragg gratings. Review article. Rev. Sci. Instrum., vol. 68, No. 12, December 1997;
7. Kenneth O. Hill and Gerald Meltz. Fiber Bragg grating technology. Fundamentals and overview. Journal of Lightwave Technology, vol. 15, No. 8, August 1997;
8. Erdogan T. Fiber Grating Spectra. Journal of Ligthwave Technology, vol. 15, No. 8, August 1997;
9. K.O.Hill, Y. Fujii, D.C. Jonson, and B.S. Kawasaki. Photosensitivity in optical fiber waveguides: Application to reflection filter fabrication. Appl. Phys. Lett., 32, 647 (1978);
10. Meltz G, Morey W, Glenn W. Formation of Bragg grating in optical fiber by the transverse holographic method. Opt. Lett. 1989;14(15), pp. 823–825;
11. Williams D.L. et al. Photosensitive index changes in germania-doped silica glass fibers and waveguides. Proc. SPIE, vol. 2044, p.55 (1993);
12. E. Pavel, I.N. Michailescu, A. Hening, and V.I. Vlad. Three-dimensional memory effect in fluorescent photosensitive glass activated by europium and cerium. Optics Letters, vol. 23, No. 16 (1998);
13. M. M. Broer, R. L. Cone, and J. R. Simpson. Ultraviolet-induced distributed-feedback gratings in Ce^{3+}-doped silica optical fibers. Optical Letters, vol. 16, No. 18 (1991);
14. Bilodeau F., Johnson D.C., Malo B., Vineberg K.A., and Hill K.O. Ultraviolet-light photosensitivity in Er^{3+}-Ge-doped optical fiber. Optics Letters, vol. 15, No. 20 (1990);
15. Gong Y., Shum P. Novel B/Ge codoped photosensitive fibers and their dispersion compensation applications. Czechoslovak Journal of Physics, vol. 51, No.2 (2001);

16. Williams D.L. et al. Enhanced UV photosensitivity in boron codoped germanosilicate fibers. Electronics Letters, vol. 29, No.1 (1993);
17. Svalgaard M. Ultraviolet light induced refractive index structures in germanosilica. Ph.D. Thesis, Mikroelektronik centret, Technical university of Denmark, 1997;
18. Lemaire P.J. Reliability of optical fibers exposed to hydrogen: prediction of long-term loss increases. Opt.Eng., vol. 30, No. 6, pp. 780-789 (1991);
19. Masuda Y. et al. Wavelength evolution of fiber Bragg gratings fabricated from hydrogen-loaded optical fiber during annealing. J. of Lightwave Technology, vol.22, No.3, pp. 934-941 (2004)];
20. Stone J. Interactions of hydrogen and deuterium with silica optical fibers: a review. J. of Lightwave Technology, vol. LT-5, No.5, pp. 712-733 (1987);
21. Helan I.R. Uniform fiber Bragg grating properties. Doctoral Degree Programme, Doctoral Degree Programme, FEEC, BUT;
22. Vasil'ev S.A. et al. Fiber gratings and their applications. Quantum Electronics, vol. 35, No. 12, pp. 1085-1103 (2005);
23. Kersey A.D. A review of recent developments in fiber optic sensor technology. Optic. Fiber Technol., vol. 2, pp. 291-317 (1996);
24. Zhao J. An object-oriented simulation program for fiber Bragg gratings. Master Thesis. 2001;
25. Giles C.R. Lightwave applications of fiber Bragg gratings. J. of Ligthwave Technol., vol. 15, No. 8, pp.1391-1404 (1997);
26. Hill K.O. et al. Chirped in-fiber Bragg gratings for compensation of optical-fiber dispersion. Optics Letter, vol. 19, No. 17, pp.1314-1316 (1994);
27. Enneser K., Ibsen M., Durkin M. Influence of nonideal chirped fiber grating characteristics on dispersion cancellation. IEEE Photonics Technology Letters, vol. 10, No.10, pp. 1476-1478 (1998);
28. Won P.C., Leng J., Lai Y. and Williams J.A.R. Distributed temperature sensing using a chirped fiber Bragg grating. Meas. Sci. Technol., vol.15, pp.1501-1505 (2004);
29. Huang S., Ohn M., LeBlanc M. and Measures R.M. Continuous arbitrary strain profile measurements with fiber Bragg gratings. Smart Mater. Struct., vol. 7, pp. 248-256(1998);
30. R.M.R. Muniz. Fiber Bragg grating structures: applications in optical communications and sensor technology. 2004;

31. K.O. Hill, B.Malo, F.Bilodeau, D.C. Johnson, and J. Albert. Bragg gratings fabricated in monomode photosensitive optical fiber by UV exposure through a phase mask. Appl. Phys. Lett., vol.62, No.10 (1993);
32. D. Basting. Excimer laser technology: laser sources, optics, systems and applications. Lambda Physik AG, First Edition, Gottingen, 2001;
33. D.J. Kitcher et al. Directional dependence of spectra of fiber Bragg gratings due to excess loss. J. Opt. Soc. Am. A, vol. 23, No.11 (2006)